

Multi-mode Plasmonically Induced Transparency in Dual Coupled Graphene-Integrated Ring Resonators

Xiushan Xia¹ · Jicheng Wang^{1,2} · Feng Zhang² · Zheng-Da Hu¹ · Cheng Liu¹ · Xin Yan¹ · Lin Yuan¹

Received: 13 February 2015 / Accepted: 24 April 2015 / Published online: 3 May 2015
© Springer Science+Business Media New York 2015

Abstract We propose a highly wavelength-tunable multi-mode plasmonically induced transparency (PIT) device based on monolayer graphene and graphene rings for the mid-IR region. The proposed PIT systems explore the near-field coupling and phase coupling between two graphene resonators. The multi-mode transparency windows in the spectral response have been observed in the graphene-integrated configurations. By varying the Fermi energy of the graphene, the multi-mode PIT resonance can be actively controlled without reoptimizing the geometric parameters of the structures. Based on the coupled mode theory and Fabry-Perot model, we numerically investigated the two kinds of coupling in the graphene-based PIT systems. This work may pave the ways for the further development of a compact high-performance PIT device.

Keywords Graphene plasmonic · Plasmonically induced transparency · Multi-mode transparency windows

Introduction

Electromagnetically induced transparency (EIT) is a special and fascinating phenomenon in laser-driven atomic systems. In EIT, the quantum destructive interference between the

excitation pathways to the atomic upper level gives a sharp transparency window within a broad absorption spectrum in the medium [1, 2]. A majority of promising applications are proposed in quantum information, nonlinear optics, ultrafast switching, slow light effect, etc. [3, 4]. Recently, the novel phenomenon analogous to EIT, which is known as plasmonically induced transparency (PIT), has been identified in various systems based on metamaterial structures [5–11]. However, in these cases, the ability to actively tune PIT resonance remains a challenge.

A monolayer graphene [12], with remarkable optical properties, such as extreme confinement, dynamic tunability [13, 14], and low losses [15], has been vigorously researched as a promising platform for plasmonics during recent years [16–21]. Particularly, the surface conductivity of graphene could be dynamically tuned by electrochemical potential via gate voltage, electric field, magnetic field, and chemical doping [22]. This increasingly promotes the development of active plasmonic devices including absorbers, polarizers, and transformation optical devices [23–25]. Liu et al. have researched a graphene-based Fabry-Perot (F-P) microcavity for plasmon-induced transparency effect [26]. Zi et al. numerically investigated EIT optical response based on graphene nanostructures [27]. Thus, monolayer graphene, which has exciting optoelectronic transport properties suitable for dynamically frequency tunable PIT planar device, is a building block for tunable sensors, switchers, and slow light devices.

In this letter, a highly wavelength-tunable multi-mode PIT device based on monolayer graphene and graphene rings for the mid-IR region has been proposed. The multi-mode transparency windows in the spectral response have been observed in our configurations composed of two graphene resonators side coupled to single-layer graphene bus waveguide. By varying the Fermi energy of the graphene, the multi-mode PIT resonance can be actively controlled without reoptimizing

✉ Jicheng Wang
jcwang@jiangnan.edu.cn

¹ School of Science, Jiangnan University, Wuxi 214122, China

² Key Laboratory of Semiconductor Materials Science, Institute of Semiconductors, Chinese Academy of Sciences, 912, Beijing 100083, China

the geometric parameters of the structure. Based on the coupled mode theory (CMT) and F-P model, we numerically investigated the near-field coupling and phase coupling in the graphene-integrated PIT systems.

Graphene Plasmonic Systems and Theoretical Model

As shown schematically in Fig. 1, the designed tunable multi-mode PIT device consists of two graphene rings and monolayer graphene. The two-dimensional numerical simulations are carried out in the configurations using the finite element method (FEM) [28]. The optical conductivity of graphene is governed by the Kubo formula including the interband and intraband transition contributions [29]. It depends on temperature T , Fermi energy E_f , momentum relaxation time τ , and photon frequency. In our analysis, the employed incident light is in the mid-infrared range where the intraband transition contribution dominates in monolayer graphene [30]. Under this condition, the optical conductivity is simplified to

$$\sigma_g(\omega) = \frac{ie^2 E_f / \pi \hbar^2}{\omega + i\tau^{-1}}, \quad (1)$$

where e is the electron charge, E_f represents the absolute value of the Fermi level and the carrier relaxation time $\tau = \mu E_f / (ev_f^2)$ relates to the carrier mobility μ , and Fermi velocity $v_f = 10^6$ m/s

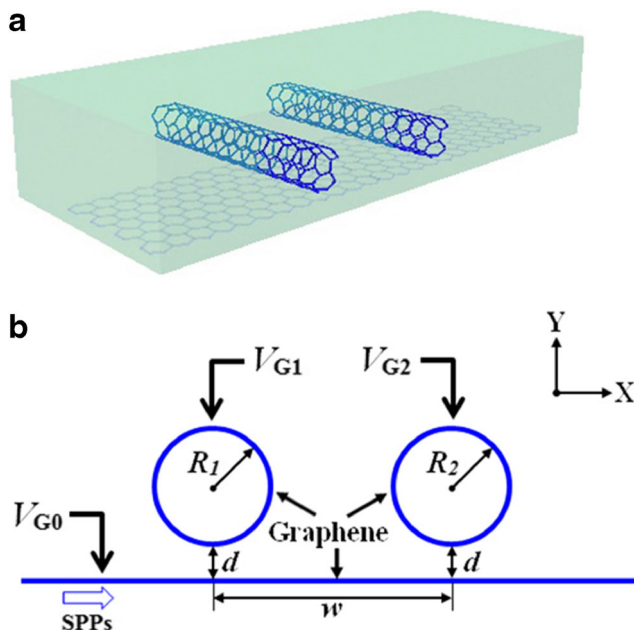


Fig. 1 Schematic of multi-mode PIT device consists of two graphene rings and monolayer graphene. **a** Three-dimensional model of the PIT device. **b** Side view of the PIT configuration: R_1 and R_2 are the radius of the two graphene rings; d is the coupling distance between the graphene waveguide and graphene rings; w is the separation between two graphene rings; V_{G0} , V_{G1} , and V_{G2} represent the gate voltages on graphene waveguide and the two graphene rings, respectively

in graphene. The equivalent permittivity of graphene is given by the equation [23] $\varepsilon_{g,eq} = 1 + i\sigma_g \eta_0 / (k_0 \Delta)$, where $\eta_0 \approx 377 \Omega$ is the intrinsic impedance of air and $k_0 = 2\pi/\lambda$ is wavenumber in vacuum.

In our simulations, the thickness of monolayer graphene and graphene ring are modeled as $\Delta = 0.5$ nm, and the carrier mobility is reasonably chosen to be $\mu = 20,000$ $\text{cm}^2 \text{V}^{-1} \text{s}^{-1}$ from experiment results [12, 24]. The TM-polarized surface plasmon polaritons (SPPs) supported by single-layer graphene is only in consideration for the investigation. The dispersion relation of this TM SPP surface wave follows the equation

$$\beta_{\text{spp}} = k_0 \sqrt{1 - \left(\frac{2}{\eta_0 \sigma_g} \right)^2}, \quad (2)$$

where β_{spp} is the propagation constant of graphene SPPs. Another important parameter derived from the above equation is the effective refractive index of graphene SPPs $N_{\text{spp}} = \beta_{\text{spp}} / k_0$, which shows the ability to confine SPPs on graphene. The propagation length is defined as $L_{\text{spp}} = 1/\text{Im}(\beta_{\text{spp}})$ featuring the SPP propagation loss in graphene. Furthermore, it should be noted that the dispersion relation of SPPs on monolayer graphene works on graphene rings as well [31]. The dependence of $\text{Re}(N_{\text{spp}})$ and L_{spp} on the Fermi level E_f and incident light wavelength λ are shown in Fig. 2. Obviously, from Fig. 2a, the $\text{Re}(N_{\text{spp}})$ increases as the Fermi level E_f decreases for a fixed wavelength, which means the SPPs are better confined at a lower Fermi level. Nevertheless, the tendency in Fig. 2b is evidently opposite to that in Fig. 2a indicating a lower Fermi level gives shorter propagation length. Thus, those two important factors should be both taken into consideration for the design of PIT systems. Interestingly, the $\text{Re}(N_{\text{spp}})$ varies greatly when the Fermi level is slightly changed, which is the guidance for active PIT device design. In this work, two PIT systems, near-field and phase coupling systems, are proposed to investigate PIT effects.

PIT Response in Near-Field Coupling Systems

At first, the near-field coupling between two graphene resonators is mainly discussed by the CMT model. The separation w has been set small so that phase coupling has less influence on the resonant frequency of the near-field coupling system. According to CMT [32], the electric field amplitudes E_1 and E_2 of the two graphene rings satisfy the following equations:

$$\frac{dE_1}{dt} = i\omega_1 E_1 + i\kappa_{12} E_2, \quad (3)$$

$$\frac{dE_2}{dt} = i\omega_2 E_2 + i\kappa_{21} E_1. \quad (4)$$

Here, κ_{12} and κ_{21} are coupling coefficients depending on the coupling distance separation w , and ω_1 and ω_2 are the

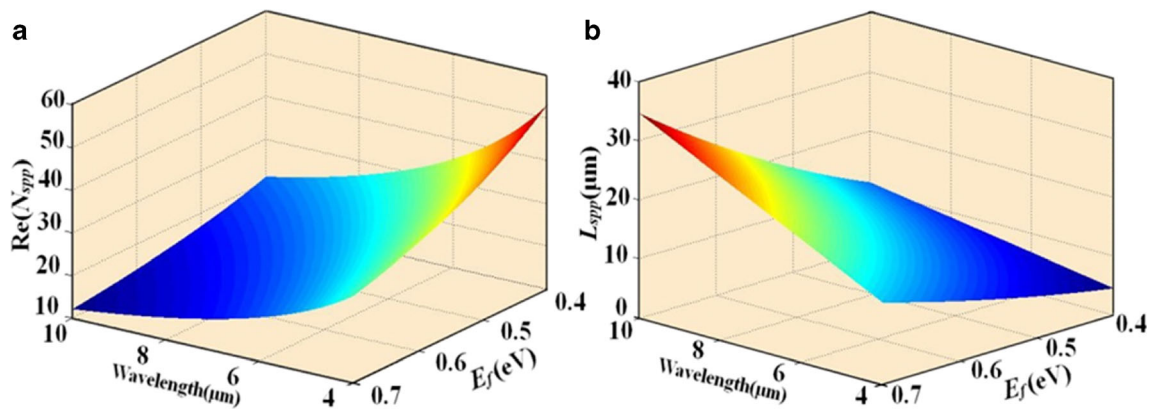


Fig. 2 **a** The real part of effective refractive index for graphene SPPs as a function of incident wavelength and Fermi level. **b** The dependence of propagation length L_{spp} on incident wavelength and the Fermi level

resonant frequency of the two graphene resonators. In the near-field coupling case, the propagation loss on the graphene waveguide between two resonators has been ignored for separation w and the $Im(\beta_{spp})$ are small enough. Based on the above equations, the PIT-resonance frequency of the near-field coupling model follows:

$$\omega = \frac{\omega_1 + \omega_2}{2} \pm \sqrt{\left(\frac{\omega_1 + \omega_2}{2}\right)^2 + |\kappa_{12}|^2}. \tag{5}$$

It is found that the resonant frequency of individual graphene resonator is split, when ω_1 equals ω_2 . The splitting frequency difference is $\Delta\omega=2|\kappa_{12}|$, which is the transparency band discussed in the following.

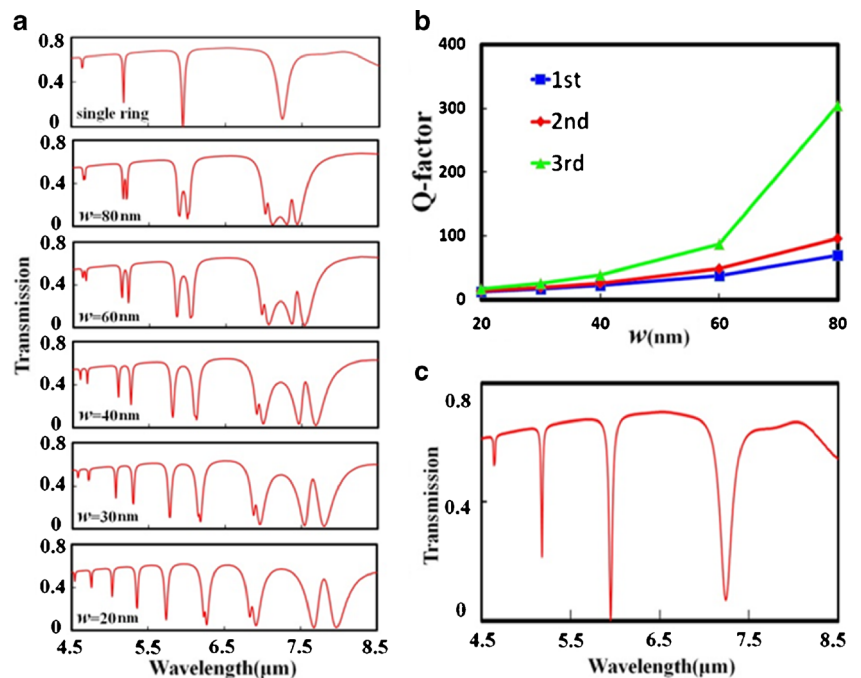
To demonstrate the PIT effect in near-field coupling system, numerical simulations have been carried out to yield its

transmission spectra with different separation w in Fig. 3a. The Fermi energy of graphene waveguide and two graphene rings are fixed at 0.4 and 0.5 eV, respectively. The coupling distance between graphene waveguide and the ring resonators is set as $d=60$ nm. From Fig. 3a, the first spectrum shows multiple pronounced dips with one graphene resonator. The resonance wavelength of SPPs on graphene ring should follow the phase-matching equation [33]:

$$Re(\beta_{spp}) \cdot 2\pi R = 2m\pi, \tag{6}$$

where m is a positive integer, resonance mode number. From the remaining subfigures in Fig. 3a, as w decreases from 80 to 20 nm, the multi-mode PIT windows present and become increasingly apparent and broad owing to the intensification of coupling between the two graphene rings. Interestingly, the

Fig. 3 **a** Transmission spectra of single-ring system and near-field coupling PIT system at different separation w . **b** The Q value of the transparent windows for first-order, second-order, and third-order modes versus separation w . **c** Transmission spectrum of PIT system with bias on the right-side ring by a gate voltage



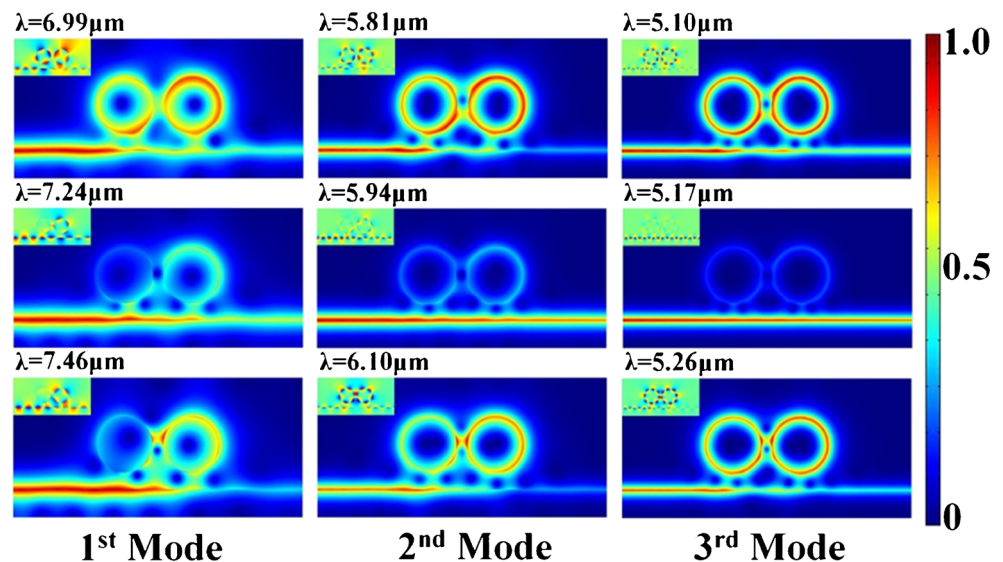
sub-PIT windows have been observed in first- and second-order resonance mode regions, and the sub-transparency peaks get more evident with the two coupling rings closer. The Q-factor of the multi-mode PIT windows is defined as $\lambda_0/\Delta\lambda$, where λ_0 and $\Delta\lambda$ are transparency-peak wavelength and full width at half maximum (FWHM) of the transparent window, respectively. As shown in Fig. 3b, the Q value increases dramatically with a growing w . It is obvious that the Q value of high-mode PIT window is more sensitive to the coupling separation w . These two important features can be employed to modulate the Q of PIT resonance. Since the optical conductivity of graphene can be tuned by gate voltage, the interference process can be actively controlled. When one of the graphene rings is biased, its Fermi energy can be correspondently varied. Supposing the gate voltage gives a Fermi energy $E_f=0.05$ eV, the biased graphene ring will no longer support SPPs because the interband transition of electrons occur at this Fermi energy [17]. According to the corresponding transmission spectrum, this system works just like the system with a single graphene ring indicating that the transparency windows of each mode can be dynamically switched on or off, shown in Fig. 3c.

To explore the physics of the observed multi-mode PIT transmission spectra, the normalized electric field distributions corresponding to the transparency windows for first-order, second-order, and third-order modes are visually illustrated in Fig. 4. When the incident wavelength $\lambda=7.24$, 5.94, and 5.17 μm , the two graphene resonators interfere destructively with each other at some specific wavelength, which results in the PIT optical response. Moreover, the destructive interference is stronger as the separation gets smaller.

PIT Response in Phase Coupling Systems

In this part, the focus is on the phase coupling of two graphene resonators. To avoid the direct interference between two resonators, the separation w has been set large enough and tunable. The other geometric parameters are chosen as follows: $R_1=R_2=60$ nm and $d=45$ nm. Based on the phase-matching equation, we know the resonance wavelength can be adjusted via gate voltage. We define the difference between resonant wavelength of individual graphene ring as $\delta_i=\lambda_1-\lambda_2$ ($i=1, 2, 3$ for each mode). Seeing from Fig. 5a, A1–C1 illustrate the transmission spectra of the individual graphene resonator. The E_{f1} of left-hand ring is fixed at 0.52 eV, which yields three resonance dips (7.86, 5.56, and 4.55 μm) corresponding to first-order, second-order, and third-order resonance modes, depicted by the red solid line. As E_{f2} of the right-side ring grows from 0.56 to 0.64 eV, the δ_i gradually increases leading to a broader gap between two resonance dips of each mode. From the other subfigures in Fig. 5a, as the δ_i grows, the first-order mode PIT window shows an obvious off-to-on feature while the second-order and third-order transparency bands are becoming broader. Another important feature for first-order mode is that a strong PIT peak is observed only at specific values of the graphene resonator inter space w . When w is far from those values, the PIT resonance transmittance peak recedes, which can be explained in the F-P (Fabry-Pérot) resonator model. The two graphene rings can be treated as two mirrors of the F-P model with respective reflection (transmission) relating to incident wavelength. The phase retardation in propagating between two graphene resonators follows $\Delta\varphi=\text{Re}(\beta_{\text{spp}})w$. As we expected, the spectral response of the PIT systems is well predicted by the simple F-P model through the individual resonator response. The corresponding

Fig. 4 Normalized electric field distribution corresponding to transmission peaks and dips in the transparent region for first-order, second-order, and third-order modes. The insets denote the corresponding Hz distribution of graphene SPPs in the PIT systems



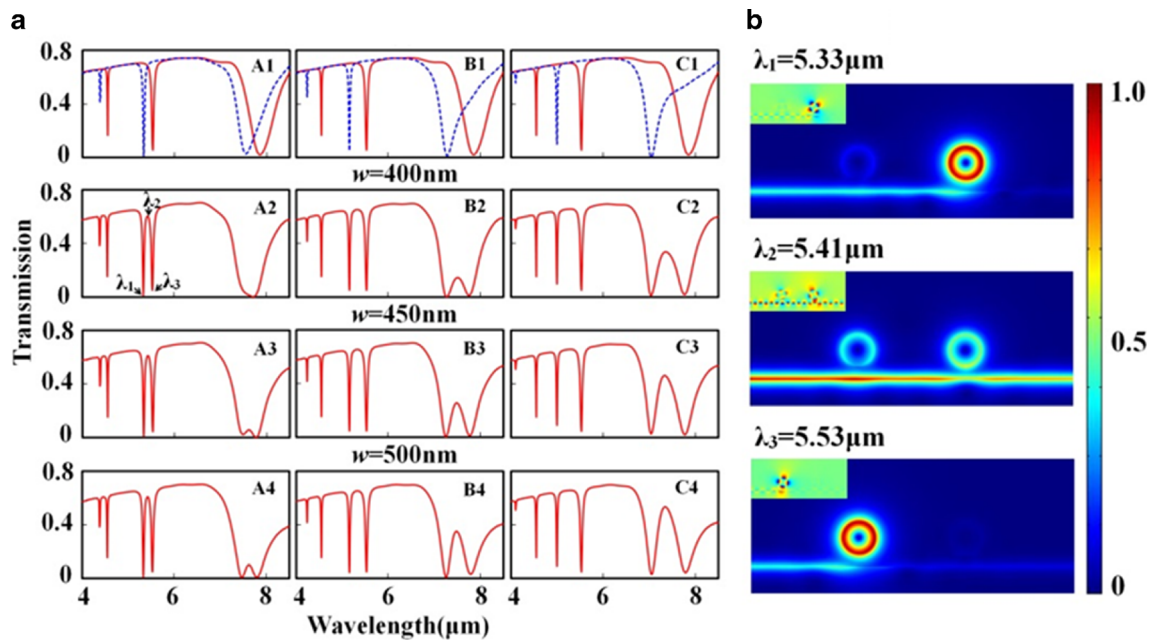


Fig. 5 **a** *A1–C1* represent the transmission spectra of the individual graphene resonator at different Fermi level. The *red solid lines* denote the transmission spectrum of the ring with Fermi level $E_{f1} = 0.52$ eV. The *blue dashed lines* show the transmission spectra of the rings with Fermi level $E_{f2} = 0.56, 0.60,$ and 0.64 eV, respectively. Subfigures 2–4 are the transmission spectra of the phase coupling PIT systems with $E_{f1} =$

0.52 eV and $E_{f2} = 0.56$ eV (*A2–C2*), 0.60 eV (*A3–C3*), 0.64 eV (*A4–C4*) for different separation, respectively. **b** Normalized electric field distributions corresponding to transmission peak and dips in the transparent region for second-order mode in A2. The *insets* denote the corresponding Hz distributions

normalized electric field at the three wavelengths from A2 in Fig. 5a visually illustrates the F-P model, shown in Fig. 5b. However, it should be noted that the size of resonator rings will introduce slight uncertainty in the value of w .

To further illustrate the off-to-on optical response of high-order mode PIT windows, we shorten the resonance difference δ_i and wavelength-sweeping region. The transmission spectra

of second-order and third-order modes are presented in Fig. 6 where the similar PIT response can be evidently observed. From the aforesaid analysis, we find high-order mode PIT window is more sensitive to the difference between resonance wavelength and high-order mode transparency peak is less sensitive to separation w , which provides guidelines for the design of a dynamical control PIT system.

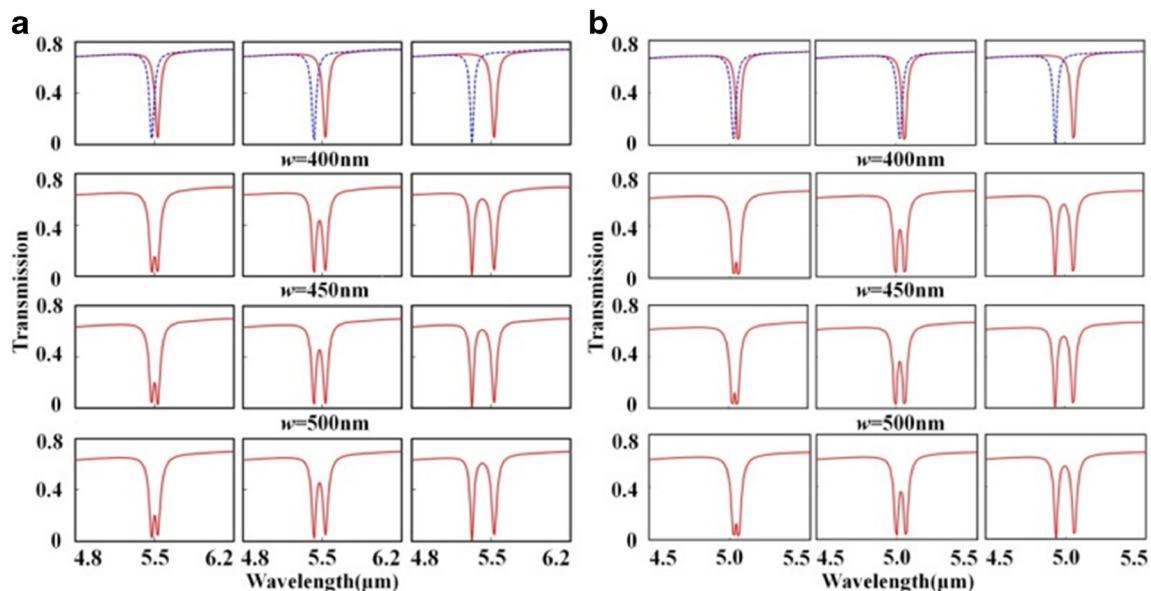


Fig. 6 **a** Off-to-on transmission spectra for second-order mode transparency window at different separation. **b** Off-to-on transmission spectra for third-order mode transparency window at different separation

Conclusion

In conclusion, we have numerically demonstrated the multi-mode PIT optical response based on monolayer graphene waveguide coupled with graphene rings for the mid-IR region. From the simulation results, the multi-mode PIT effects have been evidently observed in both near-field and phase coupling systems. In near-field coupling system, the multi-mode PIT spectral response closely depends on the coupling distance, which is well explained by CMT model. Moreover, the transparency windows of each mode can be dynamically switched on or off via varying the Fermi energy on one of the graphene resonators. For phase coupling case, the off-to-on PIT feature can be actively achieved by adjusting the resonance-wavelength difference δ_i through varying the Fermi level of graphene rings. The F-P model has been well employed to analyze the corresponding PIT spectra. It is found that high-order mode PIT window is more sensitive to the difference between resonance wavelengths and the high-order mode transparency peak is less sensitive to separation w . All of the observed PIT spectral features are of great importance to provide guidelines for the design of a dynamical control PIT system. Our work may open new ways for the further development of a compact high-performance PIT device.

Acknowledgments This paper is supported by the National Natural Science Foundation of China (Grant No. 11347196, 11404143, 61474113), the Jiangsu Natural Science Foundation (Grant No. BK20140167, BK20140128, BK2012548), the Beijing Natural Science Foundation (Grant No. 4132076), the Key Laboratory Open Fund of Institute of Semiconductors of CAS (Grant No. KLSMS-1405), the Youth Innovation Promotion Association of CAS, and the National Training Programs of Innovation and Entrepreneurship for Undergraduates of China (Grant No. 201410295027).

References

- Boller KJ, Imamolu A, Harris SE (1991) Observation of electromagnetically induced transparency. *Phys Rev Lett* 66:2593–2596
- Harris SE (1997) Electromagnetically induced transparency. *Phys Today* 50:36–42
- Krauss TF (2008) Why do we need slow light? *Nat Photonics* 2: 448–450
- Fleischhauer M, Imamoglu A, Marangos JP (2005) Electromagnetically induced transparency: optics in coherent media. *Rev Mod Phys* 77:633–673
- Zhang S, Genov DA, Wang Y, Liu M, Zhang X (2008) Plasmon-induced transparency in metamaterials. *Phys Rev Lett* 101:047401
- Liu N, Langguth L, Weiss T, Kastel J, Fleischhauer M, Pfau T, Giessen H (2009) Plasmonic analogue of electromagnetically induced transparency at the Drude damping limit. *Nat Mater* 8:758–762
- Gu J, Singh R, Liu X, Zhang X, Ma Y, Zhang S, Maier SA, Tian Z, Azad AK, Chen H, Taylor AJ, Han J, Zhang W (2012) Active control of electromagnetically induced transparency analogue in terahertz metamaterials. *Nat Commun* 3:1151
- Guo YH, Yan LS, Pan W, Luo B, Wen KH, Guo Z, Luo XG (2012) Electromagnetically induced transparency (EIT)-like transmission in side-coupled complementary split-ring resonators. *Opt Express* 20:24348–24355
- Liu X, Gu J, Singh R, Ma Y, Zhu J, Tian Z, He M, Han J, Zhang W (2012) Electromagnetically induced transparency in terahertz plasmonic metamaterials via dual excitation pathways of the dark mode. *Appl Phys Lett* 100:131101
- Cao GT, Li HJ, Zhan SP, Xu HQ, Liu ZM, He ZH, Wang Y (2013) Formation and evolution mechanisms of plasmon-induced transparency in MDM waveguide with two stub resonators. *Opt Express* 21: 9198–9205
- Wang JQ, Yuan BH, Fan CZ, He JN, Ding P, Xue QZ, Liang EJ (2013) A novel planar metamaterial design for electromagnetically induced transparency and slow light. *Opt Express* 21:25159–25166
- Novoselov KS, Geim AK, Morozov SV, Jiang D, Zhang Y, Dubonos SV, Grigorieva IV, Firsov AA (2004) Electric field effect in atomically thin carbon films. *Science* 306:666–669
- Li ZQ, Henriksen EA, Jiang Z, Hao Z, Martin MC, Kim P, Stormer HL, Basov DN (2008) Dirac charge dynamics in graphene by infrared spectroscopy. *Nat Phys* 4:532–535
- Efetov DK, Kim P (2010) Controlling electron–phonon interactions in graphene at ultrahigh carrier densities. *Phys Rev Lett* 105: 256805
- Bao QL, Loh KP (2012) Graphene photonics, plasmonics, and broadband optoelectronic devices. *ACS Nano* 6:3677–3694
- Ju L, Geng B, Horng J, Girit C, Martin M, Hao Z, Bechtel HA, Liang X, Zettl A, Shen YR, Wang F (2011) Graphene plasmonics for tunable terahertz metamaterials. *Nat Nanotechnol* 6:630–634
- Wang B, Zhang X, Yuan X, Teng J (2012) Optical coupling of surface plasmons between graphene sheets. *Appl Phys Lett* 100: 131111
- Wang B, Zhang X, Garcia-Vidal FJ, Yuan X, Teng J (2012) Strong coupling of surface plasmon polaritons in monolayer graphene sheet arrays. *Phys Rev Lett* 109:073901
- Grigorenko AN, Polini M, Novoselov KS (2012) Graphene plasmonics. *Nat Photonics* 6:749–758
- Chu HS, Gan CH (2013) Active plasmonic switching at mid-infrared wavelengths with graphene ribbon arrays. *Appl Phys Lett* 102:231107
- Fang ZY, Thongrattanasiri S, Schlather A, Liu Z, Ma LL, Wang YM, Ajayan PM, Nordlander P, Halas NJ, de Abajo FJG (2013) Gated tunability and hybridization of localized plasmons in nanostructured graphene. *ACS Nano* 7:2388–2395
- Geim AK (2009) Graphene: status and prospects. *Science* 324: 1530–1534
- Vakil A, Engheta N (2011) Transformation optics using graphene. *Science* 332:1291–1294
- Thongrattanasiri SL, Koppens FH, de Abajo FJG (2012) Complete optical absorption in periodically patterned graphene. *Phys Rev Lett* 108:047401
- Fallahi A, Perruisseau-Carrier J (2012) Design of tunable bi-periodic graphene metasurfaces. *Phys Rev B* 86:195408
- Zeng C, Guo J, Liu XM (2014) High-contrast electro-optic modulation of spatial light induced by graphene-integrated Fabry-Perot microcavity. *Appl Phys Lett* 105:121103
- Shi X, Han DZ, Dai YY, Yu ZF, Sun Y, Chen H, Liu XH, Zi J (2013) Plasmonic analog of electromagnetically induced transparency in nanostructure graphene. *Opt Express* 21:28438–28443
- Jin JM (2002) *The finite element method in electromagnetics*. Wiley-IEEE Press, New York
- Chen PY, Alu A (2011) Atomically thin surface cloak using graphene monolayers. *ACS Nano* 5:5855–5863
- Hanson GW (2008) Quasi-transverse electromagnetic modes supported by a graphene parallel-plate waveguide. *J Appl Phys* 104: 084314

31. Lu WB, Zhu W, Xu HJ, Ni ZH, Dong ZG, Cui TJ (2013) Flexible transformation plasmonics using grapheme. *Opt Express* 21: 10475–10482
32. Haus HA, Huang WP (1991) Coupled-mode theory. *Proc IEEE* 79: 1505–1518
33. Huang ZR, Wang LL, Sun B, He MD, Liu JQ, Li HJ, Zhai X (2014) A mid-infrared fast-tunable graphene ring resonator based on guided-plasmonic wave resonance on a curved graphene surface. *J Opt* 16:105004